International Journal of Nanomedicine

Dovepress

open access to scientific and medical research

Open Access Full Text Article

ORIGINAL RESEARCH

Immunomodulatory Antibacterial Hydrogel for Wound Infection Management

Jing Han[1,2,*], Qingxun Meng[1,2,*], Taicheng Liu[1,2], Mengru Lv[1,2], Wenxuan Su[1,2], Beibei Liu[1,2], Jiannan Wu[1,2]

[1]Department of Oral Implantology, Tianjin Stomatological Hospital, School of Medicine, Nankai University, Tianjin, 300041, People's Republic of China; [2]Tianjin Key Laboratory of Oral and Maxillofacial Function Reconstruction, Tianjin, 300041, People's Republic of China

*These authors contributed equally to this work

Correspondence: Jing Han; Jiannan Wu, Department of Oral Implantology, Tianjin Stomatological Hospital, School of Medicine, Nankai University, Tianjin, 300041, People's Republic of China, Email hanj0203@163.com; bdxiaosier@163.com

Background: Wound healing has always been a focal point in clinical work. Bacterial infections and immune microenvironment disorders can both hinder normal wound healing. Current wound dressings only serve a covering function. Developing wound dressings with antibacterial and immunomodulatory functions is crucial for aiding wound healing. To address this issue, we have developed a hydrogel with antibacterial and immunomodulatory functions for managing infected wounds.

Methods: The present study describes a photo-crosslinked antibacterial hydrogel composed of curcumin, silver nanoparticles-loaded reduced graphene oxide, and silk fibroin methacryloyl for the treatment of infected wounds. The study assessed its antibacterial properties and its capacity to induce macrophage M2 polarization through in vitro and in vivo experiments.

Results: The hydrogel demonstrates robust antibacterial properties and enhances macrophage M2 polarization in both in vitro and in vivo settings. Moreover, it accelerates the healing of infected wounds in vivo by stimulating collagen deposition and angiogenesis.

Conclusion: Overall, this hydrogel shows great potential in managing wound infections.

Keywords: infected wound healing, silk fibroin methacryloyl, curcumin, silver nanoparticles-reduced graphene oxide, immunomodulation, antibacterial

Introduction

Wound healing is a critical process of self-repair in the human body that involves multiple stages, including inflammation, cell proliferation, and matrix remodeling.[1] However, wound infection often hinders this process, leading to impaired healing, prolonged healing time, or scar formation. Therefore, exploring strategies to more effectively deal with wound infection and accelerate wound healing is urgent in modern medicine.[2]

Traditionally, the treatment of skin defects mainly relies on coverings such as gauze to protect the wound surface. However, this method only prevents foreign bodies from entering the wound and thus no longer meets the requirements of modern wound healing. As a new type of wound repair material, hydrogels form a unique three-dimensional (3D) network structure through physical/chemical cross-linking. They have attracted considerable attention in the field of tissue engineering owing to their excellent biocompatibility, tissue fluid absorption ability, and drug-loading capacity. For instance, type II collagen/chondroitin sulfate/hyaluronic acid hydrogel can effectively repair cartilage defects,[3] while glycosaminoglycan/methacrylated gelatin hydrogel can promote skin defect healing.[4] These studies demonstrate the good potential of hydrogels for tissue regeneration.

Silk fibroin (SF) — a natural biomaterial derived from silkworms — has attracted colossal attention due to its excellent biocompatibility, controllable biodegradability, and superior mechanical properties.[5] SF has been approved by the US Food and Drug Administration (FDA) as a safe biomaterial and is widely applied in the biomedical field. After modification by methacrylation of glycerol methacrylate, SF can be quickly dissolved in water and form an hydrogel

Received: 31 May 2024
Accepted: 31 July 2024
Published: 9 August 2024

Graphical Abstract

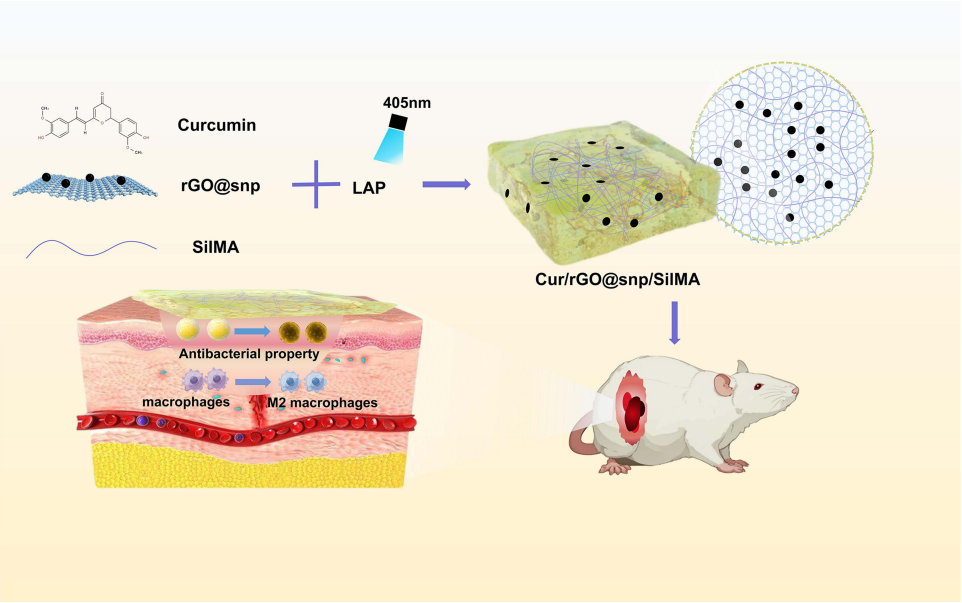

under ultraviolet (UV) light irradiation in the presence of a photoinitiator, unfolding new possibilities for its application in biomedical engineering and demonstrating its potential as an advanced biomaterial.[6]

Bacterial invasion can lead to wound infection and further affect wound healing. The classical method applies antibiotics locally or systemically in the treatment of wound infection. However, the widespread use of antibiotics often leads to the emergence of bacterial resistance. Therefore, identifying new treatment methods is urgent.[7] Silver (Ag) nanoparticles are a type of high-performance antibacterial agent, and their antibacterial effect is not only targeted towards common pathogens but also exhibits significant inhibitory effects against multidrug-resistant bacterial pathogens.[8] Nonetheless, excessively high concentrations of Ag ions have certain cytotoxicity. Graphene, a 2D nanosheet composed of sp2-carbon atoms, exhibits excellent biocompatibility and is widely used in biological field.[9] Graphene also has antibacterial properties,[10] and its introduction as a carrier of Ag nanoparticles can not only improve the antibacterial effect but also significantly reduce the cytotoxicity of Ag ions.[11] Meanwhile, introducing graphene into the hydrogel can also significantly improve the mechanical properties of the material.[12] This Ag nanoparticle/graphene composite material provides a possibility for solving the problem of bacterial resistance as a new approach to treating wound infection.

As the main bioactive component of turmeric, curcumin has a wide range of pharmacological activities, including anti-inflammatory, antioxidant, anti-tumor, and reducing scar formation.[13] Several studies have shown that curcumin can regulate macrophage polarization, steering them toward the M2 type (anti-inflammatory and reparative).[14] M2 macrophages facilitate wound healing by releasing various growth factors, recruiting cells, and promoting cell proliferation and differentiation, thus providing robust support for angiogenesis, wound healing, and tissue remodeling.[15] Inducing macrophage polarization toward the M2 phenotype represents a novel approach to enhance wound healing. However, the clinical application of curcumin is limited by various factors, such as poor water solubility and low bioavailability. Oral administration of curcumin showed that the concentration of this drug in plasma was very low.[16] Therefore, developing new strategies to effectively utilize curcumin is essential. The application of hydrogels as carriers can effectively eradicate factors limiting curcumin, providing a new approach for its wide application in medical treatment.

Simple hydrogels as dressings mostly serve only to cover wounds. Adding bioactive substances that can regulate the healing process into the hydrogels can play a positive role in wound repair. Amir et al developed a Chitosan-PVA hydrogel crosslinked with vanillin and enhanced with CuO-Ag nanoparticles to improve its antibacterial properties. This

hydrogel was demonstrated to effectively promote wound healing through its antibacterial activity.[17] Zhou et al developed a double-network hydrogel biomaterial composed of snail glycosaminoglycan (AFG) and methacrylated gelatin (GelMA), which can inhibit inflammatory factors and promote macrophage polarization to the M2 phenotype, promoted the healing of chronic diabetic wounds.[4] These studies indicate that imparting hydrogels with antibacterial and immune-regulating functions plays a positive role in inflammation and tissue remodeling during the wound healing process.

Herein, we developed a new hydrogel (Cur/rGO@snp/SilMA) with SF methacrylate as the matrix, loaded Ag nanoparticle-reduced graphene oxide and curcumin, to create a superior wound healing platform. This hydrogel not only has the advantages of convenience and moldability but also shows multi-functionality. It can effectively promote wound healing by releasing the carried curcumin and Ag ions and has the dual effects of immune regulation and antibiosis. This novel multifunctional hydrogel presents new treatment prospects to the field of wound healing and provides useful insights into the development of innovative therapeutic strategies in the future. Through further in-depth research and clinical practice, we believe that this hydrogel will play a pivotal role in the field of wound healing.

Materials and Methods

Methacrylated silk fibroin (SilMA) was obtained from (Engineering for Life, Suzhou, China). Reduced graphene loaded with Ag nanoparticles (rGO@snp) was purchased from (Kaifa New Materials, Suzhou, China). Curcumin was obtained from (Sigma-Aldrich, St. Louis, USA). All cell culture media components, including DMEM, PS, FBS, and PBS were purchased from (Thermo Fisher Scientific, Beijing, China). Cell Counting Kit 8 (CCK8) reagent was purchased from (Soleba Beijing, China), and CD206 and F4/80 antibodies were purchased from (Bioss, Beijing, China).

Preparation and Characterization of Hydrogels

Preparation of Composite Hydrogel and Hydrogel Extracts

Firstly, A 0.25% (w/v) initiator standard solution was prepared by dissolving 0.05 g of lithium phenyl-2,4,6-trimethylbenzoylphosphinate (LAP) in 20 mL of PBS using a brown vial. Subsequently, the vial was placed in a 40–50°C water bath and heated for 15 minutes with intermittent shaking for dissolution of LAP. The prepared LAP standard solution was stored at 4°C in the dark. For the preparation of a 10% (w/v) SilMA solution, 0.2 g of SilMA was weighed using a precision balance and placed in a centrifuge tube. Then, 2 mL of the prepared initiator standard solution was gradually added to the centrifuge tube, followed by stirring or shaking several times at room temperature for 0.5–1 hour to ensure complete dissolution, avoiding vigorous ultrasound, high temperatures, and strong shear. Finally, The SilMA solution was filter-sterilized using a 0.22 μm sterile syringe filter to ensure sterility. To form the SilMA hydrogel, the SilMA solution was irradiated with 405 nm ultraviolet light for 30 seconds. Next, curcumin solving in DMSO (10mM) was added to the pure SilMA solution (10%w/v) at a final concentration of 20 μM, followed by photo-polymerization to generate Cur/SilMA. Likewise, rGO@snp was added to the pure SilMA solution at a final concentration of 5 μg/mL, followed by photo-polymerization, to generate rGO@snp/SilMA. In the same manner, Cur/rGO@snp/SilMA was prepared with same concentration ratios: Curcumin (20 μM), rGO@snp (5 μg/mL). 5 mL of hydrogel was immersed in 20 mL of serum-free DMEM medium and then incubated at 37°C with 5% CO2 for 72 hours. Subsequently, the supernatant was harvested and subjected to sterilization using a 0.22 μm filter to acquire the extract, which was stored at −20°C in a light-protected environment.

Fourier Transform Infrared Spectroscopy (FTIR)

Equal amounts (2 mg) of each hydrogel (SilMA, Cur/SilMA, rGO@snp/SilMA, and Cur/rGO@snp/SilMA) were mixed individually with 100 mg of potassium bromide and ground uniformly. The mixture was pressed into a 20 MPa pellet and analyzed by a Nicolet 6700 FTIR spectrometer (Thermo Fisher Scientific, USA) at 400–4000 cm^{-1} with a 4 cm^{-1} resolution, 50000:1 signal-to-noise ratio, and 32 scans. Resulting spectra were compared to standard FTIR spectra to identify components in each sample.

Scanning Electron Microscopy (SEM)

Freeze-dried hydrogels were cut into flat sections and sputter-coated with gold for SEM imaging (Hitachi S-4800, Japan). The morphology of the cross-sections and the elemental composition of the materials were then analyzed using EDS.

Compressive Modulus Measurement

Before the compression test, the initial dimensions (length, width, and thickness) of the hydrogel samples were measured and recorded. Samples were then placed in a compression testing instrument (MTS Criterion, USA). A uniform load was applied to the samples to avoid stress concentration. The compression process was monitored and recorded, and data such as pressure, displacement, and strain were collected. The compressive modulus was calculated from the stress-strain curve. The instrument has a capacity of 0–10 kN and an accuracy of 1–100% of the load value.

Water Absorption Rate

Different dried hydrogels (M0) were immersed in PBS at 37°C. At specific time intervals, samples were retrieved, and excess surface water was gently removed using filter paper, after which their weights were measured again (M1). Each experiment was repeated three times. The water absorption rate was calculated using the following formula:

$$\text{Water absorption rate (\%)} = (M1 - M0)/M0 \times 100\%$$

Degradation Analysis

Various hydrogels were submerged in phosphate-buffered saline (PBS) until fully swollen, and their initial masses were documented as W0. Subsequently, the hydrogels were placed in a PBS solution enriched with protease (0.1 mg mL−1) at 37°C, with agitation on a shaker. At defined time points, the hydrogels were extracted from the solution and reweighed (W1). The degradation rate was determined using the formula:

$$\text{Degradation rate (\%)} = (W0 - W1)/W0 \times 100\%$$

Drug Release Analysis

Cut the Cur/rGO@snp/SilMA hydrogel into uniformly sized pieces, immerse them in 2 mL PBS, and shake them on a constant-temperature shaker at 37°C. At predetermined time intervals, withdraw a specified volume of PBS from the test tube. After each sampling, replenish with an equal volume of fresh PBS. Measure the absorbance of the sample solution at 425 nm using a enzyme-labeled instrument and calculate the concentration of curcumin using a standard curve.

Rheological Properties

The four hydrogels were placed on the stage of a rheometer (MCR92, Anton Paar, Austria). A parallel plate rotor (50 mm diameter) with a gap of 1 mm was used. The test temperature was set to 25°C. The frequency sweep was performed from 0.1 to 100 rad/s, with 25 logarithmic points and a strain of 1%.

In vitro Experiments

Cytotoxicity Assay

The CCK-8 assay and live/dead staining were used to evaluate the effect of hydrogels with different compositions on the viability of NIH-3T3 cells.

NIH-3T3 cells were incubated in 100 μL of culture medium for 24 hours. Subsequently, SilMA, Cur/SilMA, rGO@snp/SilMA, and Cur/rGO@snp/SilMA hydrogels were added to fresh culture medium, and the cells were incubated for another 72 hours, with untreated cells serving as the control group.

For the CCK-8 assay, after a further 72 hours of incubation, CCK-8 solution was added to each well, and the cells were incubated at 37 °C for an additional 4 hours. The absorbance was then measured at 450 nm.

For live/dead staining, after an additional 72 hours of incubation, calcein AM/PI working solution was added to each well. The cells were incubated in the dark for 30 minutes. The staining results were examined using a fluorescence microscope. Calcein had a maximum excitation wavelength of 494 nm and an emission peak at 517 nm. The PI-DNA complex exhibited an excitation peak at 535 nm and an emission peak at 617 nm.

Antibacterial Activity

To investigate the antibacterial activity of Cur/rGO@snp/SilMA, the extracts of hydrogels with different compositions were co-cultured with *S. aureus* and *E. coli*. The bacterial culture was extracted and diluted 1000-fold. Subsequently, 100 μL of the diluted bacterial solution was uniformly spread on Luria-Bertani (LB) plates using a cell spreader. Optical images were captured following the incubation period at 37°C for the designated duration.

RAW 264.7 Polarization Assay

Immunofluorescence staining, real-time quantitative PCR (RT-qPCR), and flow cytometry were used to evaluate the expression of M2 macrophage markers. RAW264.7 cells were seeded at a density of 2 x 10^5 cells/well into 6-well plates and cultured overnight. Subsequently, these cells were incubated with various hydrogels for 24 hours. For immunofluorescence staining, cells were incubated with CD206 antibody at 4°C overnight, and images were obtained using CLSM (Olympus, Tokyo, Japan). For RT-qPCR, all kits from (Takara, Tokyo, Japan). Primer sequences in Table 1. The results were analyzed using the 2ΔΔCt method, and GAPDH was used as a reference. For flow cytometry, flow cytometer from (Beckman, NY, USA).

In vivo Experiments

Animal Model of Infected Skin Defect

This study was conducted with the ethical approval of the Tianjin Stomatological Hospital Ethics Committee (PA2024-B-017). We followed the guidelines for the welfare of laboratory animals as specified in Guidelines for Ethical Review of Laboratory Animal Welfare (GB/T35892-2018). Full-thickness wounds with a diameter of 8 mm were created on the backs of male C57BL/6 mice using scissors. Next, 50 μL of *S. aureus* suspension (10^6 CFU/mL^{-1}) was applied to the surgical area. After 2 hours, different composite hydrogels were applied. Wound sites were photographed on days 0, 7, and 14 post-surgery to monitor healing progress.

Antibacterial Activity

The day after wound creation, bacterial samples were obtained from the wound site using a sterile cotton swab, then diluted with PBS and evenly spread on LB plates. Following a 24-hour incubation at 37°C, photographs were captured for recording purposes.

Histological Analysis

At days 7 and 14 post-surgery, mice were euthanized, and their skin tissues were collected for histological analysis. The collected tissues were then stained with hematoxylin and eosin (H&E) and Masson's trichrome staining kits (Baso, Wuhan, China) to evaluate tissue morphology and collagen deposition, respectively. Images of the stained tissues were acquired using a positive fluorescence microscope (Olympus, Tokyo, Japan).

Evaluation of M2 Macrophage Polarization and Angiogenesis Ability

Immunofluorescence staining was performed to evaluate macrophage polarization and angiogenesis status at the wound site. On day 7, the skin wound tissue was incubated with antibodies against F4/80 and CD206 for immunofluorescence staining. Immunohistochemical staining was performed using CD31. Images were acquired using a positive fluorescence microscope (Olympus, Japan).

Table 1 Primer Sequences

Gene	Primer Sequences Forward	Primer Sequences Reverse
GAPDH	5'-GAAGGTGAAGGTCGGAGT-3'	5'-GAAGATGGTGATGGGATTTC-3'
Arg1	5'-CAGAAGAATGGAAGAGTCAG-3'	5'-CAGATATGCAGGGAGTCACC-3'
CD206	5'-CAGGTGTGGGCTCAGGTAGT-3'	5'-TGTGGTGAGCTGAAAGGTGA-3'

Statistical Analysis

All experiments were performed in triplicate or more, and the data were presented as mean ± standard deviation (SD). Statistical significance was assessed using the *t*-test, with a significance level set at $p < 0.05$ (*).

Results and Discussion

Preparation and Characterization of the Hydrogel

Cur/rGO@snp/SilMA was synthesized by combining SilMA, rGO@snp, and curcumin using chemical and physical cross-linking interactions followed by UV irradiation. Figure 1A shows a macroscopic view of the Cur/rGO@snp/SilMA hydrogel. The microstructure of the hydrogel is depicted in Figure 1B, revealing a uniform and interconnected 3D porous morphology. The elemental analysis revealed a well-distributed presence of elements C, O, N, and Ag in the hydrogel (Figure 1C). Furthermore, FTIR confirmed composition and various interactions in Cur/rGO@snp/SilMA (Figure 2A). The spectral analysis identified characteristic vibrations such as O-H stretching, methyl C-H stretching, amide I, II, and III, C-O stretching, and C-H out-of-plane bending vibrations, consistent with the structure of SilMA. A comparison between the infrared spectra of Cur/SilMA and SilMA groups showed significant changes in absorption peaks at 1013 and 951 cm^{-1}, indicating chemical adsorption and successful loading of curcumin onto SilMA through chemical interactions. However, no new absorption peak or disappearance of existing peaks was observed in the infrared spectrum of the rGO@snp group compared with the SilMA group. The position and peak shape of the absorption peak remained unchanged, suggesting that reduced graphene oxide is physically adsorbed onto SilMA. The infrared spectrum of the Cur/rGO@snp/SilMA group was similar to that of the Cur/SilMA group, indicating that curcumin is chemically adsorbed onto SilMA when added with reduced graphene oxide. Moreover, reduced graphene oxide is physically adsorbed onto SilMA among proteins.

Swelling, Rheological, and Mechanical Properties of the Hydrogel

Wound healing is a complex biological process that involves a series of cellular and molecular events. In the early stages of wound healing, a blood clot forms to stop bleeding and provide a scaffold for subsequent healing. Over the next few days, the wound forms new granulation tissue, which gradually fills the wound. In the final stages, the wound forms new epithelium and regains skin integrity.[18] In the process of wound healing, dressings need to play a certain mechanical support role to help wound healing.[19] The stress-strain curves of the four hydrogels are shown in Figure 2B. The compressive strength of all four hydrogels increased gradually with increasing compressive strain. The compressive properties of the hydrogels were further measured and quantified. As shown in Figure 2C, the compressive strength of rGO@snp/SilMA and Cur/rGO@snp/SilMA hydrogels at 50% strain was 130 kPa and 140 kPa, respectively, which was similar to that of normal physiological soft tissue (100–200 kPa)[20] and significantly higher than that of pure SilMA hydrogel (20 kPa). It has been well documented that the addition of reduced graphene oxide can effectively improve the

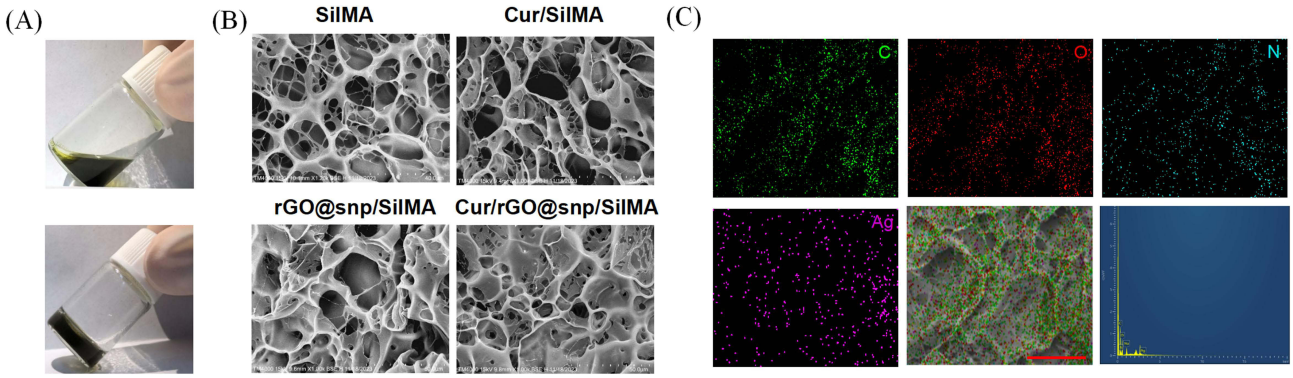

Figure 1 Morphology of hydrogels. (**A**) Photographs of the Cur/rGO@snp/SilMA hydrogel. (**B**) SEM images of various dry hydrogels. (**C**) Elemental composition of the Cur/rGO@snp/SilMA hydrogel. Scale bar: 50 μm.

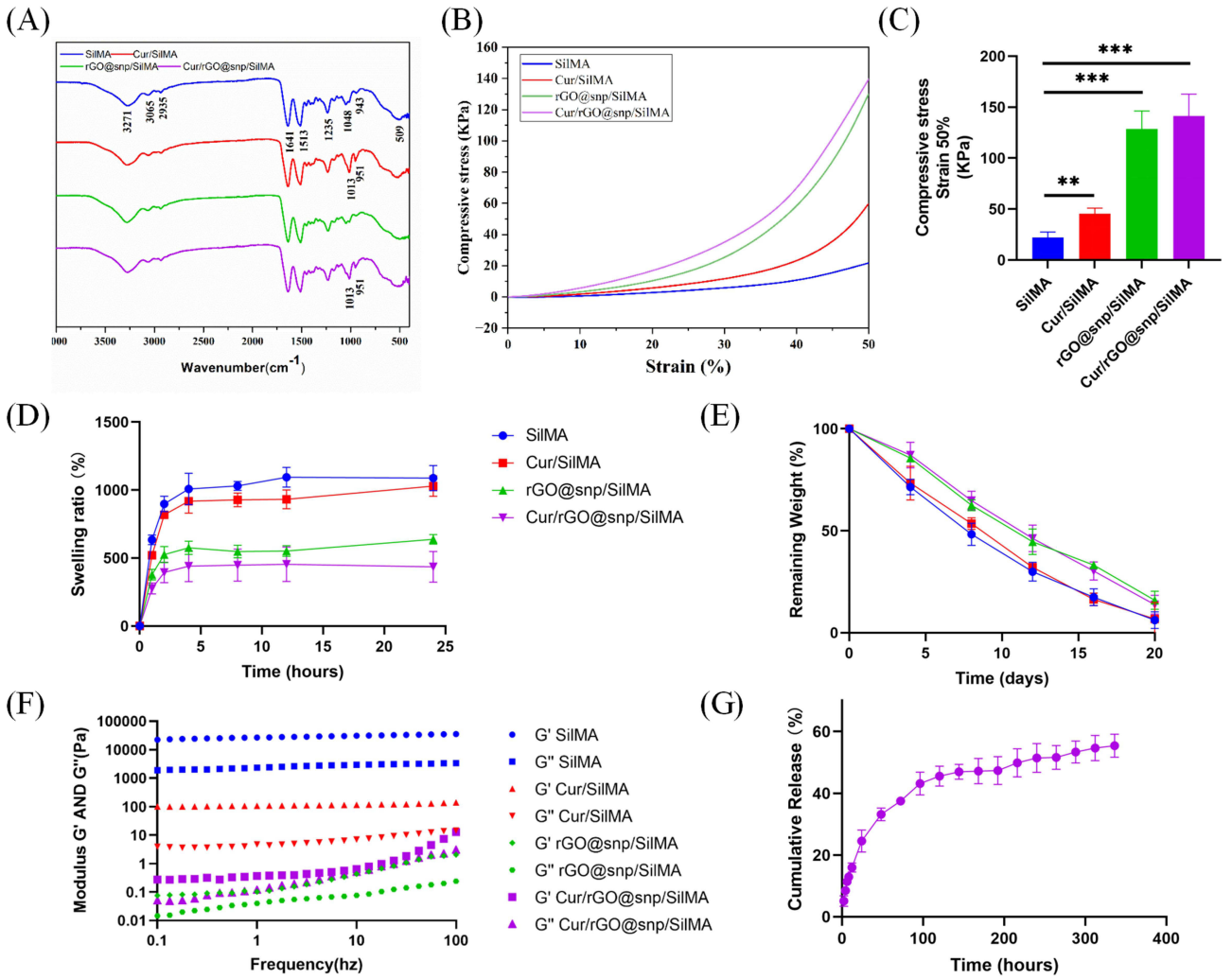

Figure 2 Characterization of hydrogels. (**A**) FTIR analysis of various hydrogels. (**B**) Stress–strain response under compression for different hydrogels. (**C**) Compressive stress of hydrogels at 50% strain (n = 3). (**D**) Swelling ratio of various dry hydrogels (n=3). (**E**) Degradation rate of different hydrogels (n = 3). (**F**) Rheological property of various hydrogels (n = 3). (**G**) The release rate of curcumin in Cur/rGO@snp/Gel (n = 3). **p < 0.01, ***p < 0.001.

mechanical properties of hydrogels.[21,22] Interestingly, the addition of curcumin alone also led to an increase in the compressive strength of the SilMA hydrogel (60 kPa). To the best of our knowledge, there is no report on the phenomenon that curcumin can improve the compressive strength of hydrogels. This phenomenon may be due to the chemical cross-linking of curcumin with methacrylated silk fibroin, which affects the internal structure of the hydrogel.

Additionally, Hydrogels were immersed in PBS for 1 days to assess their water absorption capacity, and the swelling ratio was measured based on mass increments. The results revealed rapid swelling (>250%) within the first 4 hours (Figure 2D), attributed to water molecules penetrating the gel and interacting with its hydrophilic groups, such as -OH, thereby forming a hydration layer.[23] SilMA exhibited the highest swelling ratio. The swelling ratio of Cur/SilMA was slightly lower than that of SilMA, which might be attributed to the chemical interactions between curcumin and methacrylated silk fibroin. Similarly, the incorporation of rGO@snp also reduced the swelling ratio of the hydrogel, possibly due to the increased cross-linking density of the system by the introduction of AgNPs, which could affect the water uptake ability. Additionally, the introduction of rGO, which is inherently hydrophobic, also contributed to the reduced swelling ratio.[23] Although the addition of curcumin and silver nanoparticles affected the swelling behavior of the hydrogels, the swelling ratio of Cur/rGO@snp/SilMA was still within the range reported to be suitable for wound healing applications.[24]

The degradation characteristics of the hydrogel play a pivotal role in wound healing. Increased support is essential during the initial stages to shield the newly formed tissue, whereas gradual degradation of the hydrogel in the later stages is necessary to facilitate the infiltration of new tissue into the wound site.[25] The hydrogel was immersed in PBS containing protease to evaluate its degradation rate. Upon the introduction of rGO@snp to the hydrogel, there was a deceleration in the degradation rate, possibly attributed to the diminished presence of SilMA, the primary degrading component. Throughout the 20-day experimental duration, all hydrogels exhibited degradation of at least 85% (Figure 2E), allowing ample time for diabetic wound recovery. The drug release profile within the hydrogel is also a significant property to consider. The release of Cur showcased an initial rapid increase in concentration over the first 2 days, followed by a gradual decrease, ultimately stabilizing by the 5th day (Figure 2G). Consequently, the Cur/rGO@snp/SilMA hydrogel demonstrates the capability to achieve a consistent and controlled release of Cur, ensuring sustained delivery effectiveness.

Rheological testing revealed that the storage modulus (G') of all hydrogels exceeded the loss modulus (G"), as shown in Figure 2F. This behavior indicates their elasticity. Further analysis revealed that G' slightly increased with increasing strain, and G' was always greater than G" during the whole process, indicating that the hydrogels could resist the shear of external force and maintain their state. Both the addition of curcumin and (rGO@snp) had an impact on the rheological behavior of the hydrogels.

In vitro Evaluation of Biocompatibility of the Hydrogel

Biocompatibility is a crucial factor in assessing the potential of hydrogels as biomaterials.[26] The biocompatibility of different hydrogel compositions was evaluated using the CCK8 method and live/dead staining. Different hydrogel extraction solution were incubated with NIH-3T3 cells for 72 hours, respectively. There was no statistically significant difference in OD values among the four groups, which showed that the hydrogel exhibited no cytotoxicity (Figure 3A).

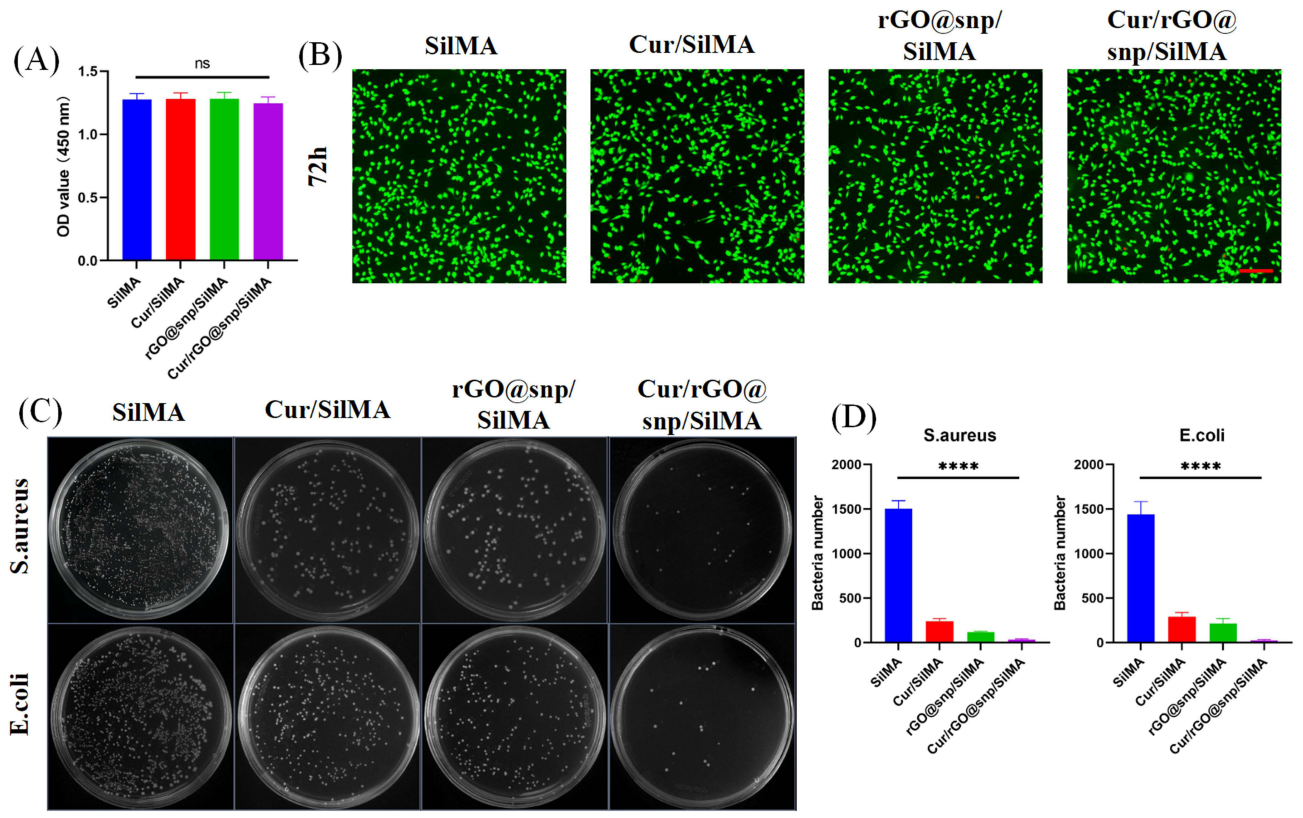

Figure 3 Evaluation of cytocompatibility and antibacterial activity of SilMA hydrogels with varying compositions. (**A**) Assessment of NIH-3T3 cells viability following 72-hour incubation with various hydrogels. (n = 3). (**B**) Live/Dead staining assessed the viability of NIH-3T3 cells cultured with various hydrogels for 72 hours. Scale bar: 500 μm (n = 3). (**C**) Evaluation of the antibacterial effects of different hydrogels against *E. coli* and *S. aureus* after 24 hours of incubation. (**D**) Quantitative analysis of colony forming units (n = 3). ns = no significant, ****p < 0.0001.

Meanwhile, Live/dead staining revealed minimal cell death all of groups, It was also confirmed that the various components of the hydrogel caused no cell death, corroborating the aforementioned findings (Figure 3B). These results collectively affirm the excellent biocompatibility of Cur/rGO@snp/SilMA hydrogel.

In vitro Evaluation of Antibacterial Properties of the Hydrogel

The skin serves as the body's primary defense against external bacterial infections. When the skin is compromised due to trauma or other factors, bacteria can enter the body through wounds, leading to infection and hindering the healing process.[27] Bacteria can also adhere to the surface of hydrogels, and potentially cause wound infections.[28] Therefore, incorporating antibacterial raw materials into hydrogels is crucial for promoting wound healing. *S. aureus* and *E. coli* are key bacteria responsible for wound infections.[29] Silver nanoparticles (AgNPs) exhibit broad-spectrum antibacterial properties by interacting with bacterial cell membranes, damaging bacterial structures, and inducing oxidative stress.[30] Curcumin — another effective antibacterial substance — disrupts cell membranes, inhibits biofilm formation, and blocks bacterial division.[31] Some studies suggest that combining curcumin with other substances can enhance antibacterial effects.[32] Testing the antibacterial properties of Cur/rGO@snp/SilMA involved soaking the hydrogel in *S. aureus* and *E. coli* culture fluids for contact sterilization experiments. As shown in Figure 3C and D, both curcumin and rGO@snp, suggesting a bactericidal effect on *E. coli* and *S. aureus*. The bactericidal effect of rGO@snp surpassed that of curcumin, aligning with previous research findings. Moreover, Cur/rGO@snp/SilMA exhibited stronger antibacterial activity compared to Cur/SilMA and rGO@snp/SilMA, indicating that both curcumin and rGO@snp exerted their respective antibacterial effects in the Cur/rGO@snp/SilMA group. Curcumin exhibits its antibacterial properties by inhibiting the assembly dynamics of filamentous temperature-sensitive protein Z (FtsZ), thereby preventing bacterial division and proliferation.[33] Silver nanoparticles have multiple antibacterial mechanisms. They effectively inhibit and kill bacteria through various pathways, including disrupting the cell membrane, generating reactive oxygen species (ROS), inhibiting protein functions, and damaging DNA.[34] Curcumin exhibits its antibacterial properties by disrupting bacterial membranes and inhibiting the shikimate pathway in bacteria. Experimental results indicate that Cur/rGO@snp/SilMA effectively sterilizes bacteria in vitro.

In vitro Evaluation of the Hydrogel Effect on Promoting M2 Polarization of Macrophages

Macrophages participates in wound healing process, particularly M2-type macrophages, which secrete anti-inflammatory cytokines, such as IL-4, IL-10, TGF-β, to reduce inflammation and facilitate healing.[35,36] Wound dressings with chemotherapeutic properties are essential for restoring immune balance during wound healing.[37]

First, the polarization of macrophages to the M2 phenotype by Cur/rGO@snp/SilMA was evaluated in vitro. Previous studies noted that M2 macrophages exhibit a more elongated morphology.[38] Key regulators of M2-type polarization include CD206 and interleukin-10 (IL-10). After 24 hours of incubation with hydrogels containing different components, RAW 264.7 cells displayed elongated morphological features in the curcumin-containing group (Figure 4A), as indicated by immunofluorescence staining for CD206. Gene expression analysis using RT-qPCR further confirmed M2 polarization of macrophages (Figure 4B), with the curcumin-added group showing significant upregulation of M2 macrophage markers such as CD206 and IL-10 ($p < 0.05$). Flow cytometry analysis of CD206 protein expression in RAW264.7 cells cultured on different hydrogels (Figure 4C and D) revealed that the Cur/SilMA and Cur/rGO@snp/SilMA groups (23.6 ± 0.65%, 22.6 ± 0.97%) exhibited significantly higher expression than the SilMA and rGO@snp/SilMA groups (12.0 ± 0.81%, 13.1 ± 1.04%), suggesting enhanced M2 polarization. Our research aligns with the conclusions of others, indicating that curcumin can regulate macrophage M2 polarization. This effect may be achieved by modulating IL-4/IL-13 levels.[14,39] However, Hydrogels containing rGO@snp did not impact M2 macrophage polarization. This may be because the rGO@snp did not come into direct contact with RAW264.7 cells, so their regulatory effects on the cells were not observed.

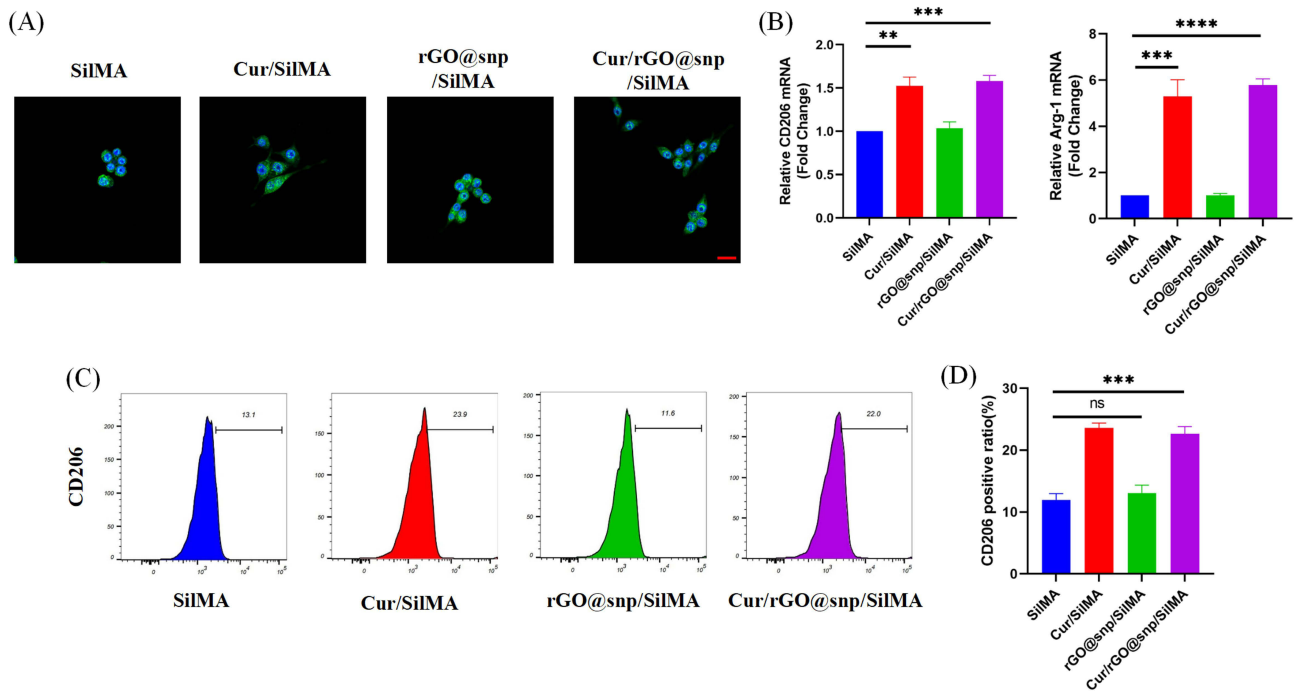

Figure 4 The effects of different hydrogels on RAW 264.7 cells morphology and M2 polarization. (**A**) Hydrogels compared for their effect on RAW 264.7 cells using immunofluorescent staining after 24-hour culture. (green: CD206; blue: cell nuclear), Scale bar: 40 μm. (**B**) RT-qPCR analysis of CD206 and Arg1 mRNA expression in macrophages. (n = 3). (**C**) Flow cytometry analysis utilized CD206-FITC staining. (**D**) Statistical analysis of CD206-positive cells (n = 3). ns = no significant, $^{**}p < 0.01$, $^{***}p < 0.001$ and $^{****}p < 0.0001$.

In vivo Analysis of the Hydrogel Effect on Skin Healing in Mice

A mouse skin defect model was established using C57BL/6 mice to assess the wound-healing properties of the hydrogel. Full-thickness skin wounds with an 8-mm diameter were created on the backs of the mice using scissors, and *S. aureus* bacteria liquid was applied to mimic wound infection. The wounds were monitored on days 0, 7, and 14, with wound tissues collected on days 7 and 14. The hydrogels were categorized into four groups based on their components (SilMA, Cur/SilMA, rGO@snp/SilMA, and Cur/rGO@snp/SilMA). As shown in Figure 5A and B), initial wound sizes were similar across all groups on day 1. However, on day 7, the SilMA group showing the highest unhealed area (40.67 ±3.54%). The Cur/rGO@snp/SilMA group exhibited the most effective healing (15.23±2.07%). The Cur/rGO@snp/SilMA group showed nearly complete healing on day 14 (0.67 ± 0.23%), while the SilMA alone group still had partial healing remaining (23.67 ± 4.74%). Bacterial infection significantly impacted wound healing, with AgNPs aiding in acceleration through their antibacterial properties. Previous studies also demonstrated that curcumin released from hydrogels at wound sites enhanced wound healing.[40] Taken together, these findings suggest that the combined effects of Cur and rGO@snp in the hydrogel enhance the healing of infected wounds.

Histopathological Evaluation

The wound healing process was assessed using H&E and Masson's trichrome staining. As illustrated in Figure 5C, the granulation tissue thickness was greater on day 7 in the Cur/rGO@snp/SilMA group than in other groups. Additionally, increased capillary growth and skin appendage recovery were observed on day 14, indicating accelerated healing effects in the Cur/rGO@snp/SilMA group. Collagen, a key component of the dermis, plays a crucial role in wound healing.[41] Collagen deposition serves as a marker for wound healing progress.[42] Masson's trichrome staining was performed across different groups to assess collagen deposition, and the results revealed a larger area of wound collagen deposition and denser collagen fibers in the Cur/rGO@snp/SilMA group (Figure 6A and B). The Cur/rGO@snp/SilMA group exhibited the largest area of collagen deposition (71.81 ± 9.72%), with dense and mature collagen fibers. The SilMA group had the least amount of newly formed collagen (28.16 ± 7.40%), while the Cur/SilMA and rGO@snp/SilMA groups had

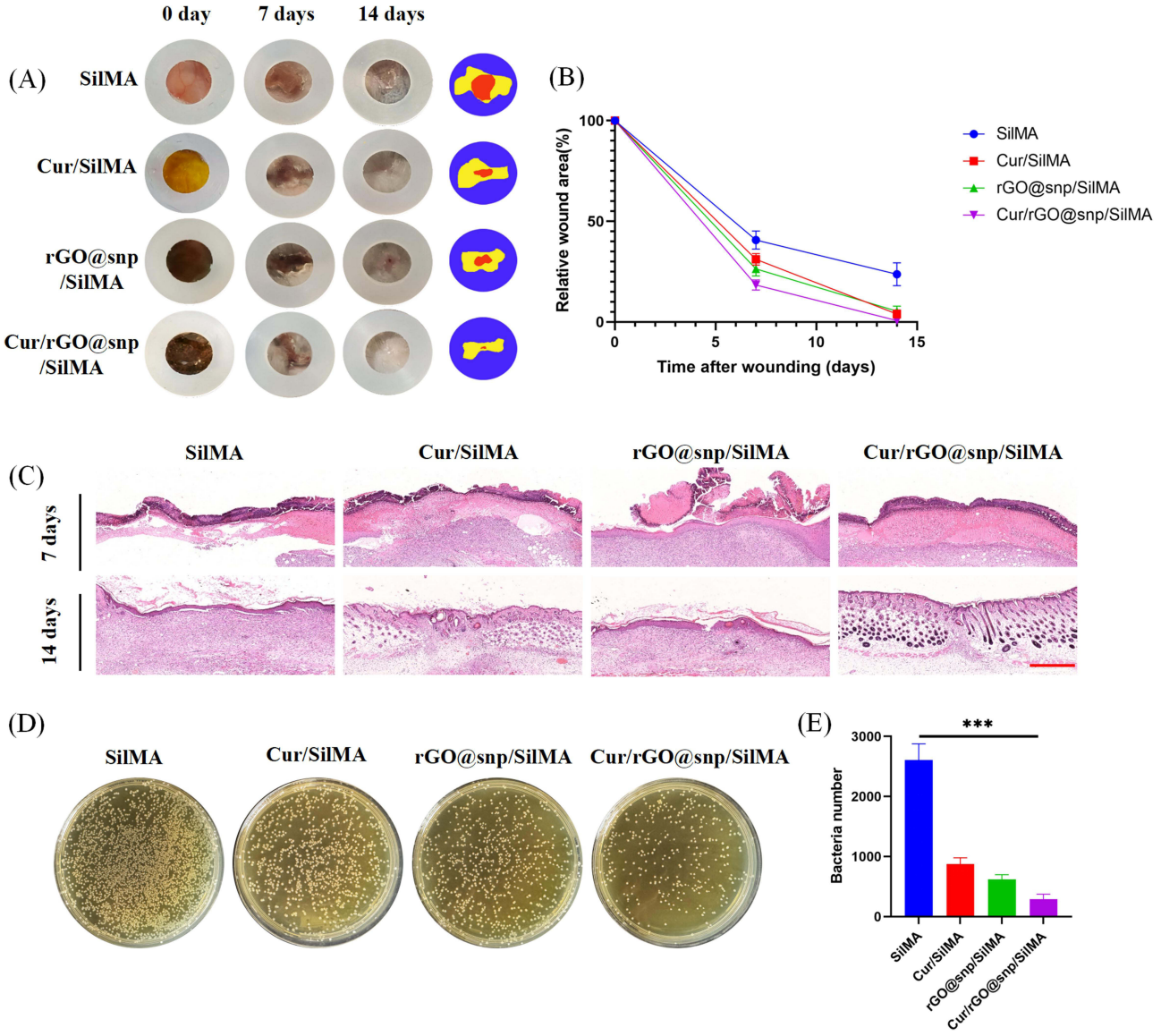

Figure 5 Comparison of hydrogel effectiveness in promoting infected wound healing. (**A**) Visual representation of the wound at days 0, 7, and 14: photographs and schematics. Internal diameter:8 mm. (**B**) Analysis of wound closure rate using quantitative methods. (n = 5). (**C**) Histological analysis of wound tissue sections treated with various hydrogels at days 7 and 14 using H&E staining. Scale bar: 400 μm. (**D** and **E**) Visual images and quantitative data showing bacterial colonies at the wound site on the second day following various treatments. ***p < 0.001.

intermediate amounts of newly formed collagen. The Cur/SilMA group had more newly formed collagen than the rGO@snp/SilMA group (59.85 ± 7.92% vs 46.41 ± 9.51%). Curcumin can effectively promote collagen synthesis, and the combination of silver nanoparticles can effectively eliminate bacteria, reduce the impact of bacteria on collagen synthesis, and accelerate the wound healing process. It can also enhance the migration of neutrophils, macrophages, and keratinocytes to the wound site, thereby promoting the regeneration of damaged skin tissue.[42]

Evaluation of Antibacterial Properties in vivo

To assess the in vivo antibacterial efficacy of the hydrogel, bacterial samples were retrieved from the skin surface two days after its application and quantitatively analyzed using the plate counting method. As illustrated in Figure 5D and E), Cur/rGO@snp/SilMA showed the most significant antibacterial effect, consistent with the findings from the in vitro antibacterial studies, emphasizing the outstanding antibacterial performance of Cur/rGO@snp/SilMA in vivo.

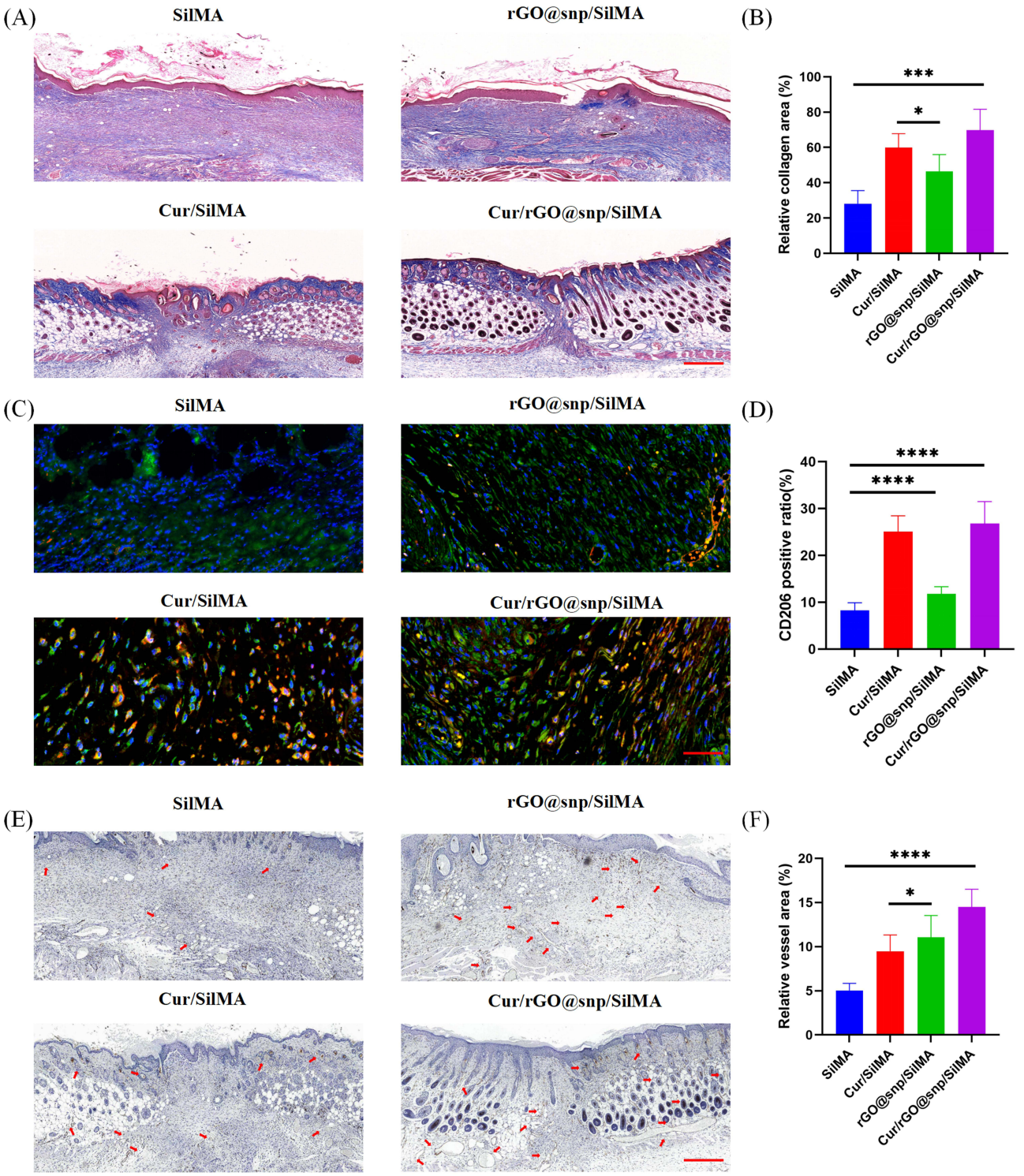

Figure 6 Evaluation of various hydrogels on collagen deposition, macrophage polarization and blood vessel formation in infected wounds. (**A** and **B**) Masson's trichrome staining was performed on day 14 (n = 5). Scale bar: 400μm. Quantitative analysis of collagen content in wound area (n = 5). (**C**) Wound tissue sections were co-stained with F4/80 and CD206 on day 7 for immunofluorescence analysis. Scalebar: 50 μm; and CD31 was visualized in wound tissue using immunofluorescence staining on day 14. Scale bar:200μm. (**D**) Three random fields per samples about ratios of the CD206-positive areas were imaged. (n = 5). (**E**) Immunohistochemical images of CD31 on the 14th day. (**F**) Quantitative analysis of CD31-positive areas (n = 5) Scale bar: 400μm. *p < 0.05; ***p < 0.001, ****p < 0.0001.

Regulation of Macrophage Polarization in vivo

Macrophages exhibit two distinct phenotypes: pro-inflammatory (M1) and anti-inflammatory (M2). Transitioning macrophages towards the M2 phenotype is considered a promising strategy for managing inflammation and promoting wound healing Our

in vitro experiments showed that the use of curcumin-containing Cur/rGO@snp/SilMA effectively promoted the polarization of macrophages towards the M2 phenotype. Subsequently, we investigated the impact of the hydrogel on M2 macrophage polarization in the context of wound healing in mice. Skin samples were collected from the mice on day 7 and immunofluorescence staining was conducted for the M2 macrophage marker protein (CD206, F4/80). It was found that the CD206 positive rate was significantly higher in the curcumin-containing group (26.68±4.22%, 24.67±3.29%) than in the curcumin-free hydrogel group (11.83±1.39%, 8.21±1.53%) (Figure 6C and D), consistent with findings from other studies. Altogether, these findings suggest that curcumin-containing hydrogel effectively modulates macrophage polarization towards the M2 phenotype during the wound healing process. In vitro experiments showed that the Cur/rGO@snp/SilMA and Cur/SilMA groups had significantly higher M2 polarization of macrophages than the other two groups, which was consistent with the results of immunofluorescence (Figure 4). Interestingly, the in vivo results showed that the rGO@snp/SilMA group had a higher CD206 positive rate than the SilMA group alone. This may be due to the fact that bacterial infection can affect the M2 polarization of macrophages,[43] and snp has bactericidal effects, which reduces the influence of bacteria on macrophages. The specific mechanism needs further study.

Regulation of Blood Vessel Formation in vivo

Angiogenesis is crucial not only for providing nutrition and managing waste during skin healing, but also for influencing cell behavior, signaling, and remodeling tissue structure.[44] When evaluating the therapeutic potential of biomaterials for treating skin defects in mice, it is essential to assess their ability to promote vascularization. Through CD31 immunohistochemistry, the degree of neovascularization can be comprehensively assessed, allowing for the analysis of blood vessel density in the skin defect area. The results showed that curcumin and silver-loaded reduced graphene oxide (rGO@snp) could effectively promote neovascularization compared with SilMA. Although the histological healing effect of the curcumin group was better than that of the rGO@snp group (Figure 6C), the rGO@snp group had a better effect on neovascularization than the curcumin group (9.02 ± 2.44% and 12.34 ± 2.85%). The Cur/rGO@snp/SilMA group showed the highest neovascularization rate (13.50 ± 2.14%) (Figure 6E and F), which also supported the results of HE staining in Figure 5C, suggesting that the two have a synergistic effect in promoting neovascularization. The results were similar to the previous HE staining results. Curcumin can promote macrophage M2 polarization, and M2 macrophages can promote neovascularization, which may be the mechanism by which curcumin promotes neovascularization.[40] As for the rGO@snp group, many studies have shown that graphene can promote neovascularization.[45] The synergistic effects of multiple components in the Cur/rGO@snp/SilMA hydrogel can better promote angiogenesis and tissue regeneration.

In vivo Evaluation of Biocompatibility of the Hydrogel

Analysis of blood parameters in mice after the application of biomaterials is a critical step in evaluating the safety, immune response, and biocompatibility of biomaterials. It is of great significance for the research and development and clinical application of biomaterials. Changes in white blood cells, hemoglobin, and platelets can be used as indicators to evaluate the overall health and safety of biomaterials in mice.[46] On day 14, the levels of white blood cells, hemoglobin, and platelets in the blood of C57BL/6 mice with skin defects treated with different hydrogels were detected throughout the treatment period to evaluate the biocompatibility of the composite hydrogels in C57BL/6 mice. The results are shown in Figure 7A. There was no significant difference in the

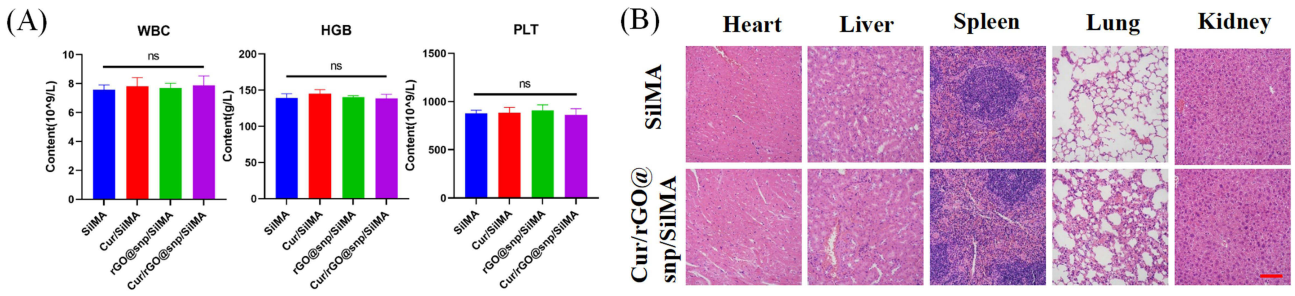

Figure 7 In vivo biocompatibility of different hydrogels. (**A**) Blood biochemical analysis and (**B**) Histological analysis of major organs using H&E staining at day 14. ns = no significant. Scale bar: 100 μm.

levels of white blood cells, hemoglobin, and platelets among the different hydrogel groups at each time point. The heart, liver, spleen, lung, and kidney are the main components of the body's metabolism, excretion, and immune system. They are important reference value for the evaluation of biocompatibility and toxicity of biomaterials. HE staining of the major organs of C57BL/6 mice did not reveal any obvious inflammatory manifestations or pathological changes. The above results show the composite hydrogel did not cause significant toxicity/verification reactions in vivo, and had good in vivo biocompatibility.

Conclusion

In conclusion, we have developed an innovative composite hydrogel termed Cur/rGO@snp/SilMA, which is formulated with curcumin, rGO@snp, and SilMA, exhibiting antibacterial and immunomodulatory properties. This hydrogel shows inhibitory activity against *S. aureus* and *E. coli* and efficiently promotes macrophages to the M2 phenotype, thus mitigating inflammatory reactions. Moreover, in vivo experiments with an infected mouse skin defect model, confirmed the hydrogel's effectiveness in enhancing the healing of infected wounds. It promoted collagen deposition and accelerated angiogenesis, thereby improving wound healing outcomes. Hence, this hydrogel emerges as a promising and ideal therapeutic agent for advancing wound healing. In summary, the present study demonstrates that Cur/rGO@snp/SilMA accelerates infected wound healing by promoting M2 macrophage polarization, inhibiting inflammation, and promoting tissue regeneration.

Abbreviations

Cur, Curcumin; rGO@snp, silver nanoparticles-loaded reduced graphene oxide; SilMA, silk fibroin methacryloyl; XRD, X-ray diffraction spectroscopy; SEM, Scanning electron microscope.

Funding

This investigation was funded by the Tianjin Health Research Project (TJWJ2022MS038), Tianjin Key Medical Discipline (Specialty) Construction Project (TJYXZDXK-048A), and National Natural Science Foundation of China (82100968).

Disclosure

The authors declare that they have no competing interests in this work.

References

1. Ferreira ADF, Gomes DA. Stem cell extracellular vesicles in skin repair. *Bioengineering*. 2018;6(1):4. doi:10.3390/bioengineering6010004
2. Turner NJ, Badylak SF. The use of biologic scaffolds in the treatment of chronic nonhealing wounds. *Adv Wound Care*. 2015;4(8):490–500.
3. Ao Y, Tang W, Tan H, Li J, Wang F, Yang L. Hydrogel composed of type II collagen, chondroitin sulfate and hyaluronic acid for cartilage tissue engineering. *Biomed Mater Eng*. 2022;33(6):515–523. doi:10.3233/BME-221404
4. Zhou Z, Deng T, Tao M, et al. Snail-inspired AFG/GelMA hydrogel accelerates diabetic wound healing via inflammatory cytokines suppression and macrophage polarization. *Biomaterials*. 2023;299:122141. doi:10.1016/j.biomaterials.2023.122141
5. DeBari MK, King CI, Altgold TA, Abbott RD. Silk fibroin as a green material. *ACS Biomater Sci Eng*. 2021;7(8):3530–3544. doi:10.1021/acsbiomaterials.1c00493
6. He X, Wang R, Zhou F, Liu H. Recent advances in photo-crosslinkable methacrylated silk (Sil-MA)-based scaffolds for regenerative medicine: a review. *Int J Biol Macromol*. 2024;256(Pt 1):128031. doi:10.1016/j.ijbiomac.2023.128031
7. Liu M, Liu T, Chen X, et al. Nano-silver-incorporated biomimetic polydopamine coating on a thermoplastic polyurethane porous nanocomposite as an efficient antibacterial wound dressing. *J Nanobiotechnology*. 2018;16(1):89. doi:10.1186/s12951-018-0416-4
8. Chinnathambi A, Alharbi SA, Joshi D, et al. Synthesis of AgNPs from leaf extract of Naringi crenulata and evaluation of its antibacterial activity against multidrug resistant bacteria. *Environ Res*. 2023;216(Pt 1):114455. doi:10.1016/j.envres.2022.114455
9. Huang X, Qi X, Boey F, Zhang H. Graphene-based composites. *Chem Soc Rev*. 2012;41(2):666–686. doi:10.1039/c1cs15078b
10. Srimaneepong V, Skallevold HE, Khurshid Z, Zafar MS, Rokaya D, Sapkota J. Graphene for Antimicrobial and Coating Application. *Int J Mol Sci*. 2022;23(1):499. doi:10.3390/ijms23010499
11. Krishnaraj C, Kaliannagounder VK, Rajan R, et al. Silver nanoparticles decorated reduced graphene oxide: eco-friendly synthesis, characterization, biological activities and embryo toxicity studies. *Environ Res*. 2022;210:112864. doi:10.1016/j.envres.2022.112864
12. Feng W, Wang Z. Shear-thinning and self-healing chitosan-graphene oxide hydrogel for hemostasis and wound healing. *Carbohydr Polym*. 2022;294:119824. doi:10.1016/j.carbpol.2022.119824
13. Shehzad A, Wahid F, Lee YS. Curcumin in cancer chemoprevention: molecular targets, pharmacokinetics, bioavailability, and clinical trials. *Arch Pharm*. 2010;343(9):489–499. doi:10.1002/ardp.200900319

14. Gao S, Zhou J, Liu N, et al. Curcumin induces M2 macrophage polarization by secretion IL-4 and/or IL-13. *J Mol Cell Cardiol*. 2015;85:131–139. doi:10.1016/j.yjmcc.2015.04.025
15. Yong L, Yu Y, Li B, et al. Calcium/calmodulin-dependent protein kinase IV promotes imiquimod-induced psoriatic inflammation via macrophages and keratinocytes in mice. *Nat Commun*. 2022;13(1):4255. doi:10.1038/s41467-022-31935-8
16. Yang C, Su X, Liu A, et al. Advances in clinical study of curcumin. *Curr Pharm Des*. 2013;19(11):1966–1973.
17. Amir F, Niazi MBK, Malik US, et al. A multifunctional vanillin-infused chitosan-PVA hydrogel reinforced by nanocellulose and CuO-Ag nanoparticles as antibacterial wound dressing. *Int J Biol Macromol*. 2024;258(Pt 1):128831. doi:10.1016/j.ijbiomac.2023.128831
18. Singer AJ, Clark RA, Epstein FH. Cutaneous wound healing. *N Engl J Med*. 1999;341(10):738–746. doi:10.1056/NEJM199909023411006
19. Ai L, He H, Wang P, et al. Rational design and fabrication of ZnONPs functionalized sericin/PVA antimicrobial sponge. *Int J Mol Sci*. 2019;20 (19):4796. doi:10.3390/ijms20194796
20. Wahlsten A, Stracuzzi A, Lüchtefeld I, et al. Multiscale mechanical analysis of the elastic modulus of skin. *Acta Biomater*. 2023;170:155–168.
21. Rehman SRU, Augustine R, Zahid AA, Ahmed R, Tariq M, Hasan A. Reduced graphene oxide incorporated GelMA hydrogel promotes angiogenesis for wound healing applications. *Int J Nanomed*. 2019;14:9603–9617. doi:10.2147/IJN.S218120
22. Jin Y, Zhang W, Zhang Y, et al. Multifunctional biomimetic hydrogel based on graphene nanoparticles and sodium alginate for peripheral nerve injury therapy. *Biomater Adv*. 2022;135:212727.
23. Sun L, Sun J, Chen L, Niu P, Yang X, Guo Y. Preparation and characterization of chitosan film incorporated with thinned young apple polyphenols as an active packaging material. *Carbohydr Polym*. 2017;163:81–91. doi:10.1016/j.carbpol.2017.01.016
24. Liu N, Zhu S, Deng Y, et al. Construction of multifunctional hydrogel with metal-polyphenol capsules for infected full-thickness skin wound healing. *Bioact Mater*. 2023;24:69–80. doi:10.1016/j.bioactmat.2022.12.009
25. Daristotle JL, Zaki ST, Lau LW, et al. Pressure-sensitive tissue adhesion and biodegradation of viscoelastic polymer blends. *ACS Appl Mater Interfaces*. 2020;12(14):16050–16057. doi:10.1021/acsami.0c00497
26. Hussein KH, Park KM, Kang KS, Woo HM. Biocompatibility evaluation of tissue-engineered decellularized scaffolds for biomedical application. *Mater Sci Eng C Mater Biol Appl*. 2016;67:766–778. doi:10.1016/j.msec.2016.05.068
27. Zomer HD, Trentin AG. Skin wound healing in humans and mice: challenges in translational research. *J Dermatol Sci*. 2018;90(1):3–12. doi:10.1016/j.jdermsci.2017.12.009
28. Eshet I, Freger V, Kasher R, Herzberg M, Lei J, Ulbricht M. Chemical and physical factors in design of antibiofouling polymer coatings. *Biomacromolecules*. 2011;12(7):2681–2685. doi:10.1021/bm200476g
29. Zhang LJ, Guerrero-Juarez CF, Hata T, et al. Innate immunity. Dermal adipocytes protect against invasive Staphylococcus aureus skin infection. *Science*. 2015;347(6217):67–71. doi:10.1126/science.1260972
30. Fatima F, Aldawsari MF, Ahmed MM, et al. Green synthesized silver nanoparticles using tridax procumbens for topical application: excision wound model and histopathological studies. *Pharmaceutics*. 2021;13(11):1754. doi:10.3390/pharmaceutics13111754
31. Dai C, Lin J, Li H, et al. The natural product curcumin as an antibacterial agent: current achievements and problems. *Antioxidants*. 2022;11(3):459. doi:10.3390/antiox11030459
32. Snetkov P, Rogacheva E, Kremleva A, Morozkina S, Uspenskaya M, Kraeva L. In-vitro antibacterial activity of curcumin-loaded nanofibers based on hyaluronic acid against multidrug-resistant ESKAPE pathogens. *Pharmaceutics*. 2022;14(6):1186. doi:10.3390/pharmaceutics14061186
33. Rai D, Singh JK, Roy N, Panda D. Curcumin inhibits FtsZ assembly: an attractive mechanism for its antibacterial activity. *Biochem J*. 2008;410 (1):147–155. doi:10.1042/BJ20070891
34. Hancharova M, Halicka-Stępień K, Dupla A, Lesiak A, Sołoducho J, Cabaj J. Antimicrobial activity of metal-based nanoparticles: a mini-review. *Biometals*. 2024;37(4):773–801. doi:10.1007/s10534-023-00573-y
35. da Silva MD, Bobinski F, Sato KL, Kolker SJ, Sluka KA, Santos AR. IL-10 cytokine released from M2 macrophages is crucial for analgesic and anti-inflammatory effects of acupuncture in a model of inflammatory muscle pain. *Mol Neurobiol*. 2015;51(1):19–31. doi:10.1007/s12035-014-8790-x
36. Gu Y, Xie X, Zhuang R, et al. A biphasic calcium phosphate cement enhances dentin regeneration by dental pulp stem cells and promotes macrophages M2 phenotype in vitro. *Tissue Eng Part A*. 2021;27(17–18):1113–1127. doi:10.1089/ten.tea.2020.0257
37. Zhu Y, Yao Z, Liu Y, Zhang W, Geng L, Ni T. Incorporation of ROS-responsive substance P-loaded zeolite imidazolate framework-8 nanoparticles into a Ca(2+)-cross-linked alginate/pectin hydrogel for wound dressing applications. *Int J Nanomed*. 2020;15:333–346. doi:10.2147/IJN.S225197
38. Li P, Hao Z, Wu J, et al. Comparative proteomic analysis of polarized human THP-1 and mouse RAW264.7 macrophages. *Front Immunol*. 2021;12:700009. doi:10.3389/fimmu.2021.700009
39. Liu X, Chen B, Chen J, et al. A cardiac-targeted nanozyme interrupts the inflammation-free radical cycle in myocardial infarction. *Adv Mater*. 2024;36(2):e2308477. doi:10.1002/adma.202308477
40. Akbik D, Ghadiri M, Chrzanowski W, Rohanizadeh R. Curcumin as a wound healing agent. *Life Sci*. 2014;116(1):1–7. doi:10.1016/j.lfs.2014.08.016
41. Bainbridge P. Wound healing and the role of fibroblasts. *J Wound Care*. 2013;22(8):407–408, 410–412. doi:10.12968/jowc.2013.22.8.407
42. Saafane A, Durocher I, Vanharen M, Girard D. Impact of ultra-small silver nanoparticles of 2 nm (AgNP(2)) on neutrophil biology: agNP(2) alter the actin cytoskeleton and induce karyorrhexis by a mitogen-activated protein kinase-dependent mechanism in vitro and transitorily attract neutrophils in vivo. *Chem Biol Interact*. 2022;365:110096. doi:10.1016/j.cbi.2022.110096
43. Mily A, Kalsum S, Loreti MG, et al. Polarization of M1 and M2 Human Monocyte-Derived Cells And Analysis With Flow Cytometry Upon Mycobacterium tuberculosis infection. *J Vis Exp*. 2020; 163. doi:10.3791/61807-v
44. Wang Z, Lu H, Tang T, et al. Tetrahedral framework nucleic acids promote diabetic wound healing via the Wnt signalling pathway. *Cell Prolif*. 2022;55(11):e13316. doi:10.1111/cpr.13316
45. Hao PC, Burnouf T, Chiang CW, et al. Enhanced diabetic wound healing using platelet-derived extracellular vesicles and reduced graphene oxide in polymer-coordinated hydrogels. *J Nanobiotechnology*. 2023;21(1):318. doi:10.1186/s12951-023-02068-x
46. Ma X, Yang S, Zhang T, et al. Bioresponsive immune-booster-based prodrug nanogel for cancer immunotherapy. *Acta Pharm Sin B*. 2022;12 (1):451–466. doi:10.1016/j.apsb.2021.05.016